Accepted Manuscript

Human Stem Cell Decorated Nanocellulose Threads for Biomedical Applications

Henrikki Mertaniemi, Carmen Escobedo-Lucea, Andres Sanz-Garcia, Carolina Gandía, Antti Mäkitie, Jouni Partanen, Olli Ikkala, Marjo Yliperttula

PII: S0142-9612(15)01008-X

DOI: 10.1016/j.biomaterials.2015.12.020

Reference: JBMT 17263

To appear in: *Biomaterials*

Received Date: 13 August 2015

Revised Date: 16 December 2015

Accepted Date: 16 December 2015

Please cite this article as: Mertaniemi H, Escobedo-Lucea C, Sanz-Garcia A, Gandía C, Mäkitie A, Partanen J, Ikkala O, Yliperttula M, Human Stem Cell Decorated Nanocellulose Threads for Biomedical Applications, *Biomaterials* (2016), doi: 10.1016/j.biomaterials.2015.12.020.

Human Stem Cell Decorated Nanocellulose Threads for Biomedical Applications

Henrikki Mertaniemi [a,†], *Carmen Escobedo-Lucea* [b,c,†,*], *Andres Sanz-Garcia*,[b,c], *Carolina Gandía*,[b] *Antti Mäkitie* [d], *Jouni Partanen* [e], *Olli Ikkala* [a,*], *Marjo Yliperttula* [b]

[a] Department of Applied Physics, Aalto University (formerly Helsinki University of Technology), P.O. Box 15100, FI-00076 AALTO, Espoo, Finland

[b] Division of Pharmaceutical Biosciences, Centre of Drug Research, Faculty of Pharmacy, University of Helsinki, Viikinkaari 5 E, P.O. Box 56, FI-00014, Helsinki, Finland

[c] Institute of Advanced Biomedical Engineering and Science, Tokyo Women's Medical University, 8-1 Kawada-cho, Shinjuku-ku, 162-8666, Tokyo, Japan

[d] Department of Otorhinolaryngology – Head and Neck Surgery, Helsinki University Central Hospital and University of Helsinki, P.O. Box 220, FI-00029 HUS, Helsinki, Finland

[e] Department of Engineering Design and Production, Aalto University, P.O. Box 14300, FI-00076 AALTO, Espoo, Finland

*Address correspondence to olli.ikkala@aalto.fi and carmen.escobedo-lucea@helsinki.fi

† H.M. and C.E.-L. contributed equally.

Abstract

Upon surgery, local inflammatory reactions and postoperative infections cause complications, morbidity, and mortality. Delivery of human adipose mesenchymal stem cells (hASC) into the wounds is an efficient and safe means to reduce inflammation and promote wound healing. However, administration of stem cells by injection often results in low cell retention, and the cells deposit in other organs, reducing the efficiency of the therapy. Thus, it is essential to improve cell delivery to the target area using carriers to which the cells have a high affinity. Moreover, the application of hASC in surgery has typically relied on animal-origin components, which may induce immune reactions or even transmit infections due to pathogens. To solve these issues, we first show that native cellulose nanofibers (nanofibrillated cellulose, NFC) extracted from plants allow preparation of glutaraldehyde cross-linked threads (NFC-X) with high mechanical strength even under the wet cell culture or surgery conditions, characteristically challenging for cellulosic materials. Secondly, using a xenogeneic free protocol for isolation and maintenance of hASC, we demonstrate that cells adhere, migrate and proliferate on the NFC-X, even without surface modifiers. Cross-linked threads were not found to induce toxicity on the cells and, importantly, hASC attached on NFC-X maintained their undifferentiated state and preserved their bioactivity. After intradermal suturing with the hASC decorated NFC-X threads in an *ex vivo* experiment, cells remained attached to the multifilament sutures without displaying morphological changes or reducing their metabolic activity. Finally, as NFC-X optionally allows facile surface tailoring if needed, we anticipate that stem-cell-decorated NFC-X opens a versatile generic platform as a surgical bionanomaterial for fighting postoperative inflammation and chronic wound healing problems.

KEYWORDS: cellulose nanofibrils, mesenchymal stem cells, wet strength, undifferentiated stem cells, surgical applications, wound healing

1. Introduction

Wound healing encompasses a series of cellular and molecular processes, such as inflammation and cell division, which act in repairing damaged tissues and re-establishing their functions. Non-effective wound healing after injury increases the risk of infection. In particular, after surgery, local inflammatory reactions as well as postoperative infections are the main causes of complications, inducing additional costs and reduced quality of life.[1,2] In some cases, the wound healing process fails and is trapped in a chronic inflammatory state. This can be especially dramatic in patients suffering from comorbidities.[3,4] Also, tissues may be vulnerable, e.g., after modern oncological treatment modalities, and recovery can be complicated by wound healing problems. The field of wound care is constantly developing new advances in pharmacological therapy.[5,6] However, none of the achievements has totally eradicated the postoperative inflammatory reaction.[7]

Human adipose mesenchymal stem cells (hASC) are regarded as an efficient and safe tool to reduce inflammation and promote wound healing, if proper administration is mastered.[1,2,8] These stem cells are attractive due to their immunomodulatory properties and their accessibility from autologous or allogeneic sources.[9] ASC have been demonstrated to promote wound healing in animal models.[2,9] Furthermore, in clinical trials, hASC have already been injected into chronic non-healing wounds with promising results, for example, in patients suffering from fistulas in Crohn's disease.[5,10] However, the efficacy of any stem cell therapy depends on the ability to deliver and retain cells at the target area under proper conditions. Cell administration by injection typically results in low cell retention, since after the procedure, the majority of the cells will

circulate via bloodstream and then deposit in other organs.[11,12] Moreover, there exists a large inter-individual variation regarding the results for the same procedure.

One way to improve the efficiency of stem cell therapies is to increase the cell retention rate in the injured area, for example, using more effective cell carriers. Potential candidates are the surgical sutures, which have already been coated with antibiotics or proteins to fight against local infection and promote healing.[13,14] Recently, a commercially available biodegradable suture, Vicryl® (polyglactin 910), has been used as a carrier for delivering ASC to the site of tracheal anastomosis in *in vivo* mice models.[2] Also, in recent *in vitro* and *ex vivo* work, hASC cultured on such sutures have been demonstrated to survive and maintain their metabolic activity after suturing.[1]

The state-of-the-art research on hASC applications in preclinical studies and surgery, including the aforementioned experiments with commercially available sutures as cell carriers, has relied on standard cell culture practices based on the use of animal-origin reagents, i.e., bovine serum. These components represent a significant potential source of pathogens, which may induce immune rejection or transmit infections.[15] The importance of the zoonosis risk in therapeutics has also been stressed by FDA and other organizations.[16] To address this problem, we have used a recently developed protocol that allows the isolation and maintenance of hASC without using animal-origin reagents, facilitating the clinical translation of new procedures or devices.[17]

In addition, the cell carrier material may affect stem cell regulation.[18] Stem cells respond to the nanoscale surface features of materials through alterations in cell adhesion.[19,20] Furthermore, material properties such as stiffness, strength and surface roughness have a crucial role in cell maintenance and differentiation. Stem cells are also sensitive to the chemical structure of the surface, for example, the type and distribution of functional groups or hydrophilic and

hydrophobic domains.[21] In this regard, the intrinsic affinity of hASC to adhere and proliferate over hydrophilic and rough surfaces has been recently reported, increasing the variety of materials to be used as culture platforms or supports for these cells.[22]

Nanofibrillated cellulose (also denoted as microfibrillated cellulose) belongs to nanocelluloses, which are nanofibers, having lateral dimensions of a few nanometers and a length up to micrometers.[23] Due to their native crystalline internal structure involving densely hydrogen-bonded parallel cellulose polymer chains, they show a high modulus of tens of GPa and a strength of 2–6 GPa.[24,25] Given their mechanical properties, sustainability, and functionalizability, NFC and nanocelluloses in general have recently attracted considerable interest towards a wide range of applications, such as reinforcement in nanocomposites, food packaging, sensor materials, aerogels, conductive structures, transparent films, and fibers.[26–34] In biomedical applications, NFC has been investigated, for example, in scaffold synthesis, stabilization of nanosuspensions in drug formulations, drug carriers, aerogels, and films.[35–38] NFC is widely available from wood and other plants, thus being particularly attractive in this context as an animal-origin-free biomaterial. In wound dressings, another type of nanocellulose, from bacterial origin, has been shown to promote healing and reduce pain.[39,40] Recently, wood-based NFC hydrogels have also succeeded in biotechnology applications such as cell culture, human pluripotent stem cell maintenance, and 3D differentiation of progenitors.[41–43] NFC forms hydrogels upon dispersing in aqueous media, and due to their strongly shear-thinning rheological properties, they can be easily extruded through a nozzle.[44]

Here, we present a new mechanically robust carrier made of extruded NFC threads for delivering hASC into injured areas. For biomedical applications with wet conditions, NFC has to be cross-linked to improve the wet strength. We show that cross-linking the NFC with

glutaraldehyde does not alter biocompability, once the resulting NFC-X threads are carefully washed. We also demonstrate that cross-linked threads are mechanically robust enough to pass through different tissues (muscle, fat and skin) – even after being exposed to cell culture conditions for more than a week. We show that hASC have a good adhesion and proliferation rate on NFC-X even without the coating with extracellular matrix (ECM) promoters. We provide evidence that the cells attached on the threads maintain their undifferentiated characteristics and immunomodulatory properties for 7–10 days, and even longer, acting as a biocompatible cell culture substrate. Finally, we demonstrate that cells remain attached to braided NFC-X threads after suturing in an *ex vivo* wound model, maintaining their metabolic activity. The complete process may be performed within a reasonable period of time considering future autologous clinical procedures preserving optimal cell quality. These results open the possibilities for a new generation of highly reproducible, zoonosis free, functionalized nanobiomaterials for biomedical applications.

2. Materials and methods

2.1. Extrusion of NFC threads

NFC (GrowDex™; UPM-Kymmene Corporation) was received from UPM as a 1.47-wt.% hydrogel, the preparation of which is described elsewhere.[41] NFC hydrogel (typically 2 ml) was extruded into an ethanol bath (200 ml) using a Fab@Home experimental 3D printer, typically with a 16G flat-tipped needle. A spiral-shaped extrusion path was used at a constant extrusion speed of 40 mm s^{-1}. The resulting gel filament had a diameter of approximately 1 mm. The gel was kept immersed in ethanol for 15 minutes to exchange water in the gel to ethanol. The filament was then transferred onto a filter paper and dried in room conditions. The resulting threads had a typical diameter of 0.1 mm.

2.2. Cross-linking of the threads

Glutaraldehyde (Sigma-Aldrich, Grade II), citric acid monohydrate (Sigma-Aldrich, 99.5–102%), sodium citrate tribasic dihydrate (Riedel-de Haën, ≥99.5%), sodium hydroxide (Sigma-Aldrich, ≥98%) and zinc nitrate (Riedel-de Haën, ≥98%) were used as received. A solution (200 ml) was prepared with 2 wt.% glutaraldehyde and 0.75 wt.% zinc nitrate, and the pH was adjusted to 4.2 with citric acid buffer (30 mM). NFC threads were immersed in the solution for an hour, then removed from the solution and cured for 30 minutes at 130°C. After this period at atmospheric pressure, the oven was pumped to a vacuum of 0.1 mbar to remove any evaporated glutaraldehyde, and evacuated immediately. The pumping-evacuating cycle took 10 minutes; thus, the samples spent a total of 40 minutes at an elevated temperature.

2.3. Tensile testing

For tensile testing, threads were cut to 20-mm pieces. To prevent slipping, each end of the thread samples was glued between two 6-mm squares of sandpaper (P600) using Loctite Precision Glue. The sample span in the tensile tester was 10 mm, and the pulling speed was 1.0 mm min^{-1}. Before and during measurement, the samples were kept at 50% relative humidity, except the threads that were soaked in water. At least six samples of each thread were measured using a Kammrath & Weiss tensile tester with a 100 N load cell. The thread cross-section area was estimated by weighing a length of NFC thread and using a literature value (1.5 g cm^{-3}) for density to calculate the cross-section. To enable direct comparison between each thread in dry and wet state, the data from wet samples is reported using the same cross-section area as their dry counterparts, and swelling is not taken into account. The experimental error estimates given with the data were calculated as 2 x the standard error of mean. The average curves shown in

Fig. 1c are constructed by first calculating the average strain at break, linearly extrapolating the datasets that break before average, and finally calculating average stress at each point.

2.4. hASC isolation and culture

Human adipose stem primary cell lines were generated from lipoaspiration procedures from healthy donors, aged between 18 and 35, following written informed consent and Research Ethical Board approval by Centro de Investigación Principe Felipe, Valencia, Spain. All the donors were previously screened for Human Immunodeficiency Virus, hepatitis C and other infectious diseases. hASC were isolated and maintained following the protocol described by Escobedo-Lucea et al.[9] After reaching the confluence, the cells were harvested with Tryple™ (Invitrogen) and seeded on the threads. In order to detect the presence of 60 different Mycoplasma species, PCR was performed using Universal Mycoplasma Detection Kit (ATCC). The reactions were carried out after hASC isolation and routinely during the cell culture in our laboratory, with negative results.

2.5. Cell seeding on NFC and NFC-X threads

After synthesis, the threads were washed at 4°C degrees in sterile PBS during 72 hours. Washing buffer was replaced by fresh for ten times. After drying, threads were sterilized by autoclave. Sterile NFC and NFC-X were optionally coated with laminin or CELLstart substrate (Life Technologies) during 2 hours at 37 °C and distributed in individual wells on Costar® Ultralow Attachment cell culture plates. The threads were maintained in sterile hASC culture media before cell seeding. In order to determine the optimal cell seeding concentration, different densities were tested: 25,000, 50,000, 100,000, 200,000 and 500,000 cells per cm of thread. Every other day, the threads where transferred to a new well and the floating cells remaining in the old ones were counted. Based on this estimation as well as the cell attachment observed by

DAPI nuclear staining, a density of 200,000 cells/cm was selected. In case of normal controls cultured on plastic (Falcon), an analogous density (cells per squared centimeter) was seeded following hASC growth ratio established earlier.[17] Medium was also changed every other day. Experiments were conducted after 7 or 10 days in culture at 37°C and 5% CO_2. All studies were performed with four hASC lines (n=4).

2.6. Scanning electron microscopy (SEM)

Samples were fixed at 37°C in 2.5% glutaraldehyde for 30 minutes. Then, threads containing cells were washed carefully 4 times with PBS, fixed and contrasted with 1% osmium during 1 hour. After washing in distilled water, samples were dehydrated in alcohol gradient. Once in 70% alcohol specimens were dehydrated through critical point treatment under controlled conditions with CO_2, 31°C, and 73 atm in an Autosamdri machine. SEM images were taken on a SEM-FEG Hitachi S-4800 equipment (University of Valencia, Spain).

2.7. Transmission electron microscopy (TEM)

For fine ultrastructural analysis, the hASC adhered on the thread were serially washed in a 0.1 M phosphate buffer (PB; pH 7.4) solution, prior to their fixation for TEM. Fixation was performed in 3% glutaraldehyde solution in PB for 30 minutes at 37°C and postfixed in 2% OsO4 in PB. Dehydration was achieved by a graded series of ethanol solutions and a final rinse with propylene oxide (Lab Baker, Deventry, Holland). Finally, samples were embedded in araldite (Durkupan, Fluka) overnight. Following polymerization, embedded samples were detached from the chamber slide and glued to Araldite blocks. Serial semi-thin (1.5 µm) sections were cut with an Ultracut UC-6 (Leica, Heidelberg, Germany), mounted onto slides and finally stained with 1% toluidine blue. Ultrathin (0.07 µm) sections were prepared with the Ultracut and stained with lead citrate. Photomicrographs were obtained under a transmission electron

microscope (FEI Tecnai Spirit G2), using a digital camera (Morada, Soft Imaging System, Olympus).

2.8. Cell attachment over NFC-X thread: in vivo microscopy experiments

Microdrop culture technique was used for the analysis of hASC attachment over the NFC-X threads. Briefly, the monofilament threads were placed inside 35-mm Hydrocell low attachment culture plates (CellSeed). These plates avoid cell attachment on their surface; thus, the only surface allowing attachment would be the thread. The hASC could only attach between themselves or over the thread. hASC were detached, counted and their cytoplasm was stained with 5 µl of Vybrant DiL (Catalog number: V22855 Thermo Scientific) to facilitate their visualization under the in vivo confocal microscopy assay. Vybrant Dil staining was performed following the instructions from the provider. A 20-µl micro-droplet of culture media containing 7500 cells was dispensed over the thread, and covered with mineral oil for embryo culture (Sigma-Aldrich) to prevent evaporation. The cultures were incubated at 37°C and 5% CO_2 inside a Sanyo incubator equipped with an Olympus LCV100 incubation imaging confocal system. The evolution of the cultures was recorded for 24 hours. Dil was imaged using a 561-nm laser.

2.9. TUNEL assay and cell staining

Click-iT TUNEL imaging assay (Life Technologies) was used to detect percentage of apoptotic cells, according to manufactured instructions. Briefly, the cells were fixed with 4% PFA in PBS followed by a permeabilization with 0.25% TritonX-100. The next step was the TdT incorporation of EdUTP into double strain DNS strand breaks, followed by fluorescent detection of EdUTP with click chemistry. The nuclei were counterstained with DAPI and α-tubulin (Sigma-Aldrich) or CD90 were used to stain cell cytoplasm. Positive control apoptotic hASC

were prepared by incubation with DNAse according with provider's recommendations. All the samples were examined under confocal microscopy (Zeiss).

2.10. Assessment of cell proliferation using WST-8 tetrazolium salt

Cell survival was assessed by 2-(2-methoxy-4-nitrophenyl)-3-(4-nitrophenyl)-5-(2,4-disulfophenyl)-2H-tetrazolium(WST-8) assay. NFC, NFC-X, and Nylon threads were cutted in 5-mm pieces and placed inside a low attachment 96-well plate (CellSeed). The number of viable hASC seeded per well was 10.000 cell/mL. WST-8 assay was carried out in four independent experiments using Cell Count Reagent SF, based on WST-8 (Nacalai Tesque, Kyoto, Japan) according to the manufacture's instructions. Absorbance at 450 nm was measured in a SpectraMax® M2e multimode microplate reader and SoftMax® Pro Software (Molecular Devices) at 1, 3, 5, and 7 days after culture. The influence of phenol red and tetrazolium was removed by subtracting the absorption value of a blank solution from the absorption value of each well.

2.11. Detection of hASC proliferation by Ki-67 expression.

Briefly, 10^5 cells were seeded per each 1-cm monofilament threads of NFC and NFC-X to detect cell proliferation. The same number of cells was seeded on glass culture chambers. After incubation at 5% CO_2 and 37°C for 24 h and 36 h, cultures were fixed with 4% paraformaldehyde (PFA) at room temperature for 10 minutes and permeabilized by incubation with 0.1% Triton X-100 in PBS for 15 min and then blocked for 1 hour at room temperature with a buffer solution composed of 1% Bovine Serum Albumin (BSA) and 0.3M Glycine in 0.1% Tween (all from Sigma-Aldrich). Subsequently, cultures were incubated with a monoclonal antibody against KI-67 directly conjugated with APC (dilution 1:50; Milli-Mark cat. number FCMAB103AP) at 4°C overnight. Then, samples were washed with 0.1% Tween in PBS. Actin

filaments were stained by incubation with Phalloidin Alexa 488 (Dilution 1:50; Thermo Scientific) at room temperature for 15 minutes, and washed five times with PBS. Coverslips were affixed to glass slides using Prolong® Diamond antifade reagent containing DAPI (Thermo Scientific). Fluoresce images were captured using an Olympus FV1200 confocal microscope (Tokyo, Japan).

2.12. RT-PCR analyses

hASC seeded on NFC and NFC-X threads were analyzed for CD90, CD73, CD166, CD29, CD44, CD45, perilipin (PLIN), adiponectin and adducing 1 (ADD1), using RT-PCR techniques and specific primers.[17] Undifferentiated hASC, human peripheral Blood Mononuclear Cells (hPBMC) and commercial cDNA from human fat (hFAT) (Stratagene) were used as positive controls. Total RNA was extracted using the RNeasy kit (Qiagen) following manufacturer's instructions and treated with DNAse (Qiagen). Total RNA obtained was checked by spectroscopy using NanoDrop 2000c Spectrophotometer (Thermo Scientific) to assess the quantity and purity acquired. An A_{260}/A_{280} ratio between 1.8 and 2.0 was deemed optimal to accept the sample for experimental procedures. Total RNA was then converted to cDNA through reverse transcription using the High Capacity cDNA Reverse Transcription Kit (Applied Biosystems). The reaction mixture contained 2 µg RNA, 2 µL RT buffer 10X, 2 µL random primers 10X, 0.8 µL dNTPs and 1 µL enzyme, and DEPC H_2O to reach a final volume of 20 µL . PCR using the synthesized cDNA was performed to determine the presence or absence of different transcripts using an Eppendorf PCR machine with β-2-microglobulin as internal control.

2.13. RT-qPCR studies

For quantitative real-time PCR (QRT-PCR), 5 µg of RNA was converted into cDNA, and a series of diluted samples were used for 40-cycle PCR with Light Cycler 480 SYBR Green I Master (Kit no. 04707516001) in a Lightcycler 480 (Roche Diagnostics, Mannheim) instrument. Reactions (20 µL in total) contained 1 µL cDNA, 10 µM each primer, and 4 µM probe; and were run using the default Lightcycler 480 program. Standard curve using multiple dilutions of the control cDNA sample were generated to check the primers, determine the optimal conditions and threshold values. Individual samples were analyzed in triplicate using the probe of interest and an internal control expected to be unchanged between samples (an undifferentiated hASC line). From the Ct values, the relative expression ratio (*R*) of an unknown sample versus the control was determined, and expressed in comparison to that of the housekeeping/reference gene β-2 microglobulin.

2.14. Detection of differences in cytokine secretion by Protein Array

We compared the differences on the cytokine release pattern of cells seeded over plastic and over NFC-X. The experiment was performed twice using a total of six hASC lines in pools of two samples (n=3).

Seven days after seeding, cultures were washed three times with Hank´s balanced salt solution (HBSS, Life Technologies) and media was replaced by basal mesenchymal culture media for 24 hours. After this time the supernatant was collected, centrifuged at 400g for 5 min (to remove cell debris) and stored at -80°C until analysis. A control containing media without cells was included in order to detect and normalize the concentration of cytokines in the culture media. The porosity of the thread could, in principle, increase the retention of proteins; thus, culture media without cells maintained with NFC-X was also introduced as an additional control

condition. The controls (n=1) were obtained after 24h incubation of the basal media added to the NFC-X and plastic.

To determine the cytokine profile, the cytokine (human) antibody array AA0077 (Abnova) was used following the instructions from the provider. Pixel integrated density was determined using ImageJ software.[45] Normalized expression levels were calculated using the positive spots and the background and converted into relative values dividing every condition (NFC-X without cells, hASC on plastic, and on NFC-X threads) by the controls (plastic without cells).

2.15. Surgical "hands on" mechanical strength testing using pig tissue

NFC and NFC-X decorated tensile testing *in vivo* were performed at the Centro de Investigación Principe Felipe (CIPF) in three female Large White pigs. Animals were used for non-related surgery educational programs non-related with this project; Animals were previously housed trying to reduce the stress by transport, and anesthetized. After 12 h of solid starvation the animals were sedated through intramuscular administration of 10 mg kg^{-1} Dexmedetomidine (Dexdomitor, Esteve, Barcelona, Spain) and Azeperone (Strespil, Esteve, Barcelona, Spain). Anesthesia was then induced by intravenous administration of 1% Lipuro (BBRaun, Vetcare, Barcelona, Spain), through a 22 G catheter placed in the ear's lateral vein, in a dose-response regimen (2–3 mg kg^{-1}) to allow proper endotracheal intubation. In addition, the animals were connected to an anesthetic machine (Primus®, Draeger Medical) and anesthesia was maintained with sevofluorane (Sevorane®, Abbott Laboratories, Madrid, Spain) (2.7% in 1 l min^{-1} O_2) through a circular circuit attached to a ventilator (Ohmeda 7800, Datex Ohmeda, Helsinki, Finland). Surgical analgesia was achieved through the administration of fentanyl (Fentanest, Kernpharma, Barcelona, Spain) at an infusion rate (0.3 µg kg^{-1} h^{-1}). Animals were closely monitored by hemodynamic and ventilator parameters during surgery. During the educational

procedure, they were subjected to anastomosis and intestinal resections principally; thus, those procedures did not affect our testing or results. Once finalized the surgical training and before euthanasia induction by pentobarbital overdose, our "hands-on" tests were performed.

2.16. Survival of cells after suturing "ex vivo" pigskin samples with multifilament sutures

For this analysis, multifilament sutures (n=5), were prepared by braiding NFC-X threads manually in groups of 8 or 7 filaments. Once prepared, hASC (2×10^6) were seeded in 9-cm sutures, following the protocol described by Reckhenrich et al.[1] After one week in culture, the hASC decorated sutures were passed intradermally three times through *ex vivo* pigskin. Then, these sutures and their controls were cut in 1cm pieces and placed in 96 well plates. Mitochondrial metabolic activity of the cells remaining in the sutures was examined after the process and 24 hours later by incubation with WST-8 (tetrazolium salt, Nacalai Tesque) for 3–4 hours at 37°C. This assay is based in the extracellular reduction of WST-8 by NADH produced in the mitochondria. The levels of reduced compound were measured using a Spectramax M2e microplate reader (Molecular Devices) at 450 nm. Cell morphology was studied in detail using TEM following the protocol previously described. The corresponding suture controls were also included in the study.

3. Results and discussion

3.1. Mechanical strength of NFC under wet conditions was increased by chemical cross-linking

Threads of nanofibrillated cellulose were prepared by utilizing a modified Fab@Home Model 2 3D printer to extrude NFC hydrogel into an ethanol coagulation bath, followed by drying in air (Figure 1a). The diameter of the resulting threads could be tuned by the nozzle chosen and the

speed in the extrusion setup. Threads with a diameter of 0.1 mm and 0.2 mm were typically made (Figure1b). The NFC threads had a tensile strength of 275 MPa, an elastic modulus of 13 GPa, and a strain at break of 9.5% in the dried state (Figure 1c). This result indicates that the native NFC used in this study forms particularly ductile structures in comparison to the previously reported NFC fibers and films.[33,34,46–49] The results of tensile tests in dried state are summarized in Table 1.

However, under the wet hydrated state, relevant for surgical applications, the NFC threads have unacceptably low mechanical strength (Table 1). Thus, in order to improve the wet strength of NFC macrofibers, the threads were chemically treated with glutaraldehyde, which covalently cross-links NFC nanofibers.[50] In the dry state, the mechanical properties of these cross-linked NFC threads (NFC-X) were quite similar to the non-modified NFC threads, as shown in Figure 1c. The cellulose nanofibrils bind strongly together with a dense network of hydrogen bonds, and the additional covalent bonds from the cross-linking by glutaraldehyde made the NFC-X threads slightly more brittle without significantly affecting the elastic modulus. In contrast, the cross-linking resulted in a pronounced improvement on the mechanical properties in the wet state, where the hydrogen bonding between cellulose nanofibers is disturbed by water. Therein, the NFC-X threads soaked in water were able to retain up to 40% of the dry-state tensile strength of NFC, resulting in a wet strength in the range of strongest human tendons.[51] Furthermore, the elongation at break of NFC-X decreased only slightly when soaked in water. Intriguingly, the NFC-X threads consist of intertwining cross-linked NFC nanofibers, and the architecture resembles “nanoyarns” (Figure 1c). Importantly, the washing procedure allowed removing the potentially unbound glutaraldehydes, rendering good biocompatibility, to be discussed shortly. Despite of their lower strength, NFC threads were maintained as controls in the following

experiments to evaluate cell adhesion and biosafety of NFC itself, without the glutaraldehyde treatment.

3.2. NFC-X threads can be passed through different tissues

In order to evaluate the manipulation of the threads in a more practical setting, "hands-on" testing was performed. To recreate necessary conditions required for hypothetical *in vivo* studies, hASC were seeded on NFC and NFC-X threads and maintained at 37°C, 95% humidity and 5% CO_2. After one week embedded in culture media and exposed to hASC metabolism, threads were tested in muscle, dermis and epidermal layers in both *post-mortem* and *in-vivo* pig tissues during a non-related surgical procedure. The results indicate that whereas non-modified NFC was too weak to be handled after 7 days under cell culture conditions (Video S3), NFC-X was much stronger, and the monofilament thread could be pulled through skin and manipulated *in vivo* and also in *post-mortem* tissues. Tests with NFC-X are shown in Videos S4 and S5. These results further imply that our approach enables the cellulosic material to be removed from the body if required.

3.3. Stem cells attach and divide on the nanocellulose threads

To test the affinity of hASC for the threads prepared, the cells were cultured over NFC and NFC-X for 7 days. The process is illustrated in Figure 2a. Figure 2b shows SEM micrographs of the threads before cell seeding. Note that NFC and NFC-X threads are composed of porous nanofiber networks with topological features having similarities to the ECM (additional details in Fig. S2a).

After seeding, the cells attached on both NFC and NFC-X surfaces (Figure 2c). In contrast to their counterparts on NFC, which show a non-homogeneous distribution, hASC grew more homogeneously along the surface of the NFC-X threads: whereas the cells attached to NFC were observed to be round and small, hASC on NFC-X assumed an elongated fibroblast-like shape, characteristic of mesenchymal cells.[17,52] This observation highlights the importance of the surface roughness and topographical features of the material in cell adhesion and growth (Figure S4). Cell adhesion was also confirmed by cytoplasmic actin filament staining using phalloidin. Cell nuclei were counterstained with 4´,6-Diamidino-2-phenylindole (DAPI). The results (Figure 3, and Videos S1 and S2) show that hASC were able to attach on the thread surfaces. Generally, the characteristic elongated fibrillar features shown by phalloidin staining were more profuse for hASC seeded on NFC-X than on NFC (Figure 3a). Figure 3b shows transversal 3D projections of hASC decorated threads showing their cytoplasm stained with CD90 and nuclear TO-PRO®, further illustrating the attachment and distribution of growing hASC on the surface of threads.
The cell adhesion over NFC-X mono-filaments was also recorded and analyzed. Videos S6 and S7 show that during the first 2 hours of culture, cells start to form aggregates that are able to attach and colonize the surface of the material. The cells continue attaching even after 24 hours.

It is important to note that hASC have a good adhesion on NFC-X even without the coating with extracellular matrix (ECM) promoters, which are usually required for other artificial scaffolds. However, if required, the dense set of surface hydroxyl groups on NFC allows facile chemical modification to additionally fine-tune the bioadhesion.

Additionally, cell proliferation over NFC and NFC-X was assessed by the detection of Ki-67 expression using immunocytochemistry (Figure 4a) and also through the analysis of mitochondrial activity using WST-8 (tetrazolium salt) reduction. Figure 4b shows the evolution

of the metabolic activity of the hASC on both types of threads for one week. Cells were able to grow over NFC, NFC-X or Nylon without significant differences after 7 days in culture. Cultures over plastic were also included in the assay. As expected, the hASC exhibited higher proliferation ratio on plastic than over the threads due to the higher area available for growth and the specific culture treatment (Data not show but available upon request).

3.4. Glutaraldehyde cross-linking of NFC did not induce toxicity on hASC

The biocompatibility of the NFC hydrogel has been reported before.[41–43] In this work, the nanocellulose material was cross-linked with glutaraldehyde for improved wet strength. However, even though glutaraldehyde is commonly used in the preparation of medical bioprostheses and protein stabilization, it has been reported that this aldehyde may be released from some cross-linked biomaterials inducing toxicity.[53,54] To remove glutaraldehyde from NFC-X threads, the threads were washed repeatedly for 72 hours before cell seeding. To exclude the possible cytotoxicity induced during the *in vitro* cultivation with the threads, transmission electron microscopy (TEM) analysis of cell ultrastructure (Figure 3c) and terminal deoxynucleotidyl transferase-mediated (dUTP) nick-end-labeling (TUNEL) assay studies[55] were performed (Figure 3d). TEM studies show that, in all conditions, all nuclei exhibited packed chromatin and well developed nucleoli (Fig. 3c and S6a). Regarding the abundance of cytoplasm organelles and their feature, no differences between NFC, NFC-X threads, or their counterparts over plastic were detected. Mitochondria were elongated with prominent cristae, which corresponds to cells with normal metabolic functions.[56] Rough endoplasmic reticulum (rER) appeared covered by ribosomes. Smooth endoplasmic reticulum (sER) was well organized and not dilated. Cellular signals compatible with toxicity as phagocytic vesicles, swollen or abnormal

mitochondria or autophagy vacuoles were absent in cells over NFC and NFC-X. Altogether, the detailed morphology studies indicated the absence of toxicity traces in the cells after their culture on the NFC-X threads.[57]

The quantification of apoptotic cell death assay was performed by TUNEL (Figure 3d, S7a and S8). We observed extremely low overall percentages of TUNEL-positive cells undergoing apoptosis after one week in culture: NFC, 2.25 ± 0.11; NFC-X, 2.21 ± 0.26; control, 1.54 ± 0.12 (mean ± SEM). There was no statistically significant difference in the number of cells between the NFC, and NFC-X groups (n=4, $p > 0.05$). The results confirmed that the washing steps performed before the cell seeding were adequate to reduce residual traces of glutaraldehyde to a non-toxic level.

3.5. NFC-X threads maintain hASC undifferentiated profile and functionality

Stem cell differentiation can be triggered by culture over certain surfaces or other alterations in the surrounding niche.[58] Importantly, the immunomodulatory properties of hASC diminish until disappear during stem cell differentiation process towards terminally differentiated cell types. Therefore, after ten days in culture, cells over the NFC-X threads were monitored by RT-PCR for transcriptional evidence of genes associated with undifferentiated state of mesenchymal stem cells (CD90, CD73, CD166, CD29, CD44). On the other hand, to detect differentiation processes, we assessed the lack of expression of hematopoietic gene marker CD45 as well as some genes involved in adipocyte maturation PLIN, adiponectin and ADD. Beta-2-microglobulin was introduced as housekeeping gene (Figure 5a). Quantitative PCR for these genes confirmed the absence of differences between the cells cultured over plastic and on the NFC-X (Figure 5b). Additionally, CD90 expression in cell cytoplasm was also traced using

immunocytochemistry (Figure 5c). After ten days in culture over NFC-X, hASC maintained their mesenchymal undifferentiated profile. Taking into consideration the future use of NFC-X threads in clinical practice, seven to ten days would be a reasonable time window for the extraction of autologous or heterologous cells and their delivery in optimal conditions. However, hASC maintained in an undifferentiated state in the presence of nanocellulose and cross-linked nanocellulose for longer than 4 passages during a series of experiments not related to this work (data not shown but available under request).

Undifferentiated mesenchymal stem cells secrete a broad panel of growth factors and cytokines with trophic, immunomodulatory, antiapoptotic and proangiogenic properties. However, this paracrine profile varies according to their initial activation by different stimuli.[59] To assess cell functionality after culture, the effect of the NFC-X threads on the hASC bioactivity was studied *in vitro*. Protein array analysis was conducted for 60 cytokines that intervene in several different processes as immunomodulation, angiogenesis or differentiation (see Table S1 for the full list of cytokines) to detect possible changes on the cytokine pattern released from the hASC after their contact with the NFC-X. The position of the cytokines in the array is shown in Figure S11. A level of cytokine expression detected in each condition was compared using plastic without cells as control.

Figure 6a and 6b show the comparison between the paracrine cytokine pattern secreted by the hASC over NFC-X and their counterparts maintained on plastic. To assess the effect of NFC-X (without cells) on the cytokine pattern, the culture media was incubated for 24h with an NFC-X thread. The cytokines present in the basal media were the same in both conditions; plastic or NFC-X without cells. After the array exposition, a slightly lower signal intensity was perceived for IGFBP3 (3C) and VEGF-D (5J) (Figure 6b, white bars). The differences may be due to the

porosity of the nanocellulose material. Apart from these we consider that the incubation with NFC-X it is not altering the composition of the basal culture media, allowing the comparison of the cytokines secreted by hASC on plastic or over NFC-X.

The cytokine pattern secreted by hASC after one week in culture was similar on both plastic and NFC-X. However, hASC maintained over plastic released high levels (<2-fold changes) of Osteoprotegerin, IGFBP6, GRO, TIMP2 and TIMP-1, while hASC cultured over NFC-X secreted relevant amounts (<1.5-fold changes) of FGF-4, VEGF-D, IGFBP3, G-CSF, IL12P40, Angiopoietin-2, AgRP, Fas-TNFRSF6 but specially IL-8 (10-fold changes), ACRP30(5-fold changes), μPAR and ENA-78 (<2-fold changes each one).

Even though cytokines are not the only molecules involved in tissue regeneration and immunomodulation processes, our results indicate that the culture over NFC-X does not induce major changes in the pattern of molecules secreted. On the contrary, cytokines involved in immunomodulation and wound healing are secreted by hASC over NFC-X in high levels as demonstrated by the signal detected for IL-8, which modulates inflammation and reduces wound contraction,[1] Acrp30, an anti-inflamatory adipokine,[60] μPAR, involved in plasminogen activation, tissue regeneration and wound healing,[61] or ENA-78 that regulates neutrophils and has also angiogenic properties.[62] The full list of cytokines showing different expression between NFC-X and plastic, as well as their function is shown in Table S2. From the point of view of the future potential of the stem-cell-decorated NFC-X threads on immunomodulation and wound healing processes, these results show that the bioactivity of mesenchymal stem cells was not compromised after the culture over the NFC-X thread. Our results are consistent with previous work that has shown an unchanged pattern of angiogenic cytokines involved in wound healing released by hASC after their culture on Vicryl® sutures.[1]

3.6. The NFC-X fibers can optionally be surface modified in order to tune cell binding

It was shown above that NFC-X threads support cells attachment and growth, maintaining their undifferentiated properties, without the need to involve any additional surface treatments on the threads. Next, we show that the NFC-X fibers can be optionally biofunctionalized. Since artificial bioscaffolds are often coated using extracellular matrix (ECM) proteins to promote cell binding, we also tested coating the threads with human laminin (LM) and CELLstart™(CS) to optionally tune the cell adhesion by adding specific interactions with the cells.[63] The results show that the nanofibrous surface morphology of NFC-X was maintained after the coating (Figure S2b). Cells over coated NFC-X threads were found to spread across the thread similarly to the non-coated surfaces, implying an apparently good material–cell adhesion (Figure S3, S4, and S5). The optional coatings were also found to support the undifferentiated state (Figure S9).

3.7. Cells on decorated NFC-X multifilament threads remain attached after suturing.

In order test if the cells would remain viable in nanocellulose sutures after a suturing process, an *ex vivo* suturing assay was performed using NFC-X multifilament threads. After one week in culture, decorated NFC-X sutures were pulled through pig skin three times. The quantity of cells remaining in the sutures after the procedure was indirectly measured through the reduction of tetrazolium salt by their mitochondria. Figure 7 shows the comparison between metabolic activity of the cells remaining in the decorated NFC-X sutures after crossing the skin and their controls. The mitochondrial metabolic activity of hASC in the threads was lower after the suturing, suggesting that some cells are damaged or detached during the process. However, the differences between the controls and the sutures pulled through skin were not significant 3.5 hours after the procedure. In order to detect variations caused by cell death after the possible

damages, the sutures were maintained in culture and the measurements were repeated. The results show that 24 hours after the procedure, the metabolic activity in both groups of sutures increased. The reduction of tetrazolium salt seems lower in samples pulled through the skin than in controls, but none of the detected differences is statistically significant (Figure 7a). This is consistent with previous observations in a study where hASC were cultured on Vicryl® sutures.[1] Finally, cell morphology after suturing was analyzed using TEM (Figure 7b), further confirming that cells survived the suturing.

4. Conclusions

Threads of nanofibrillated cellulose were fabricated and decorated with human adipose mesenchymal stem cells, which have been shown to improve wound healing if properly administered. To increase their strength under wet conditions, NFC threads were chemically modified using glutaraldehyde, resulting in the highest wet strength reported for NFC-based materials. The hASC, isolated and maintained without the use of animal-origin reagents, were capable to homogeneously attach and grow on the cross-linked threads, even without additional coating components. The NFC-X threads supported cell growth without altering their characteristics or inducing toxicity. The time required for the hASC to reach culture confluence on the threads is reasonable (7 days); thus, it would be feasible to prepare the cells from the patient's own adipose tissue before surgery. Ultrastructural and metabolic studies performed after *ex vivo* surgical tests using multifilament NFC-X sutures confirmed that hASC remained on the material after passing through the tissue three times. The cells maintained their mitochondrial metabolic function and their morphology was comparable to normal functional cells.

We see these results opening new possibilities in personalized medicine. In particular, hASC decorated NFC-X provides a xenogeneic-free tool for delivering stem cells into injured areas in a

precise manner that might be useful to reduce postoperative inflammation and help in the treatment of chronic wounds, expanding the possibilities of NFC in biomedical applications.

Acknowledgments

This work was partially funded by TEKES-The Finnish Academy of Innovations, Academy of Finland Research Fellowship, Academy of Finland based on the Center of Excellence of Molecular Engineering of Biosynthetic Hybrid Materials Research, academy professorship, and a European Research Council Advanced Grant Mimefun. C.E.L. and A.S.G. are funded by Academy of Finland under Research Fellow Program (num. 266486) and the FINSKIN Project associated (num. 273689), respectively. This work made use of the Central services of the University of Valencia (SCSIE) and CIPF – Valencia. We would like to thank Mrs. Teresa Minguez, Mrs. Viviana Bisbal, Dr. Tatsuya Shimizu, Professor Teruo Okano, Dr. Masayuki Yamato Dr. Vicente Mirabet, Dr. Deborah Burks, Professor J.M. Garcia-Verdugo and Dr. M Angeles Asensi for their technical support.

References

(1) Reckhenrich, A. K.; Kirsch, B. M.; Wahl, E. A.; Schenck, T. L.; Rezaeian, F.; Harder, Y.; Foehr, P.; Machens, H.-G.; Egaña, J. T. Surgical Sutures Filled with Adipose-Derived Stem Cells Promote Wound Healing. *PLoS One* **2014**, *9*, e91169.

(2) Georgiev-Hristov, T.; García-Arranz, M.; García-Gómez, I.; García-Cabezas, M. A.; Trébol, J.; Vega-Clemente, L.; Díaz-Agero, P.; García-Olmo, D. Sutures Enriched with Adipose-Derived Stem Cells Decrease the Local Acute Inflammation after Tracheal Anastomosis in a Murine Model. *Eur. J. Cardiothorac. Surg.* **2012**, *42*, e40–e47.

(3) Aranguren, X. L.; Verfaillie, C. M.; Luttun, A. Emerging Hurdles in Stem Cell Therapy for Peripheral Vascular Disease. *J. Mol. Med. (Berl).* **2009**, *87*, 3–16.

(4) Amos, P. J.; Kapur, S. K.; Stapor, P. C.; Shang, H.; Bekiranov, S.; Khurgel, M.; Rodeheaver, G. T.; Peirce, S. M.; Katz, A. J. Human Adipose-Derived Stromal Cells Accelerate Diabetic Wound Healing: Impact of Cell Formulation and Delivery. *Tissue Eng. Part A* **2010**, *16*, 1595–1606.

(5) García-Olmo, D.; García-Arranz, M.; García, L. G.; Cuellar, E. S.; Blanco, I. F.; Prianes, L. A.; Montes, J. A. R.; Pinto, F. L.; Marcos, D. H.; García-Sancho, L. Autologous Stem Cell Transplantation for Treatment of Rectovaginal Fistula in Perianal Crohn's Disease: A New Cell-Based Therapy. *Int. J. Colorectal Dis.* **2003**, *18*, 451–454.

(6) Tozer, P. J.; Burling, D.; Gupta, A.; Phillips, R. K. S.; Hart, A. L. Review Article: Medical, Surgical and Radiological Management of Perianal Crohn's Fistulas. *Aliment. Pharmacol. Ther.* **2011**, *33*, 5–22.

(7) Murphy, P. S.; Evans, G. R. D. Advances in Wound Healing: A Review of Current Wound Healing Products. *Plast. Surg. Int.* **2012**, *2012*, 190436.

(8) Teng, M.; Huang, Y.; Zhang, H. Application of Stems Cells in Wound Healing-an Update. *Wound Repair Regen.* **2013**, *22*, 151–160.

(9) Puissant, B.; Barreau, C.; Bourin, P.; Clavel, C.; Corre, J.; Bousquet, C.; Taureau, C.; Cousin, B.; Abbal, M.; Laharrague, P.; *et al.* Immunomodulatory Effect of Human Adipose Tissue-Derived Adult Stem Cells: Comparison with Bone Marrow Mesenchymal Stem Cells. *Br. J. Haematol.* **2005**, *129*, 118–129.

(10) Lee, W. Y.; Park, K. J.; Cho, Y. B.; Yoon, S. N.; Song, K. H.; Kim, D. S.; Jung, S. H.; Kim, M.; Yoo, H.-W.; Kim, I.; *et al.* Autologous Adipose Tissue-Derived Stem Cells Treatment Demonstrated Favorable and Sustainable Therapeutic Effect for Crohn's Fistula. *Stem Cells* **2013**, *31*, 2575–2581.

(11) Barbash, I. M.; Chouraqui, P.; Baron, J.; Feinberg, M. S.; Etzion, S.; Tessone, A.; Miller, L.; Guetta, E.; Zipori, D.; Kedes, L. H.; *et al.* Systemic Delivery of Bone Marrow-Derived Mesenchymal Stem Cells to the Infarcted Myocardium: Feasibility, Cell Migration, and Body Distribution. *Circulation* **2003**, *108*, 863–868.

(12) Guyette, J. P.; Fakharzadeh, M.; Burford, E. J.; Tao, Z.-W.; Pins, G. D.; Rolle, M. W.; Gaudette, G. R. A Novel Suture-Based Method for Efficient Transplantation of Stem Cells. *J. Biomed. Mater. Res. A* **2013**, *101*, 809–818.

(13) Li, Y.; Kumar, K. N.; Dabkowski, J. M.; Corrigan, M.; Scott, R. W.; Nüsslein, K.; Tew, G. N. New Bactericidal Surgical Suture Coating. *Langmuir* **2012**, *28*, 12134–12139.

(14) Fuchs, T. F.; Surke, C.; Stange, R.; Quandte, S.; Wildemann, B.; Raschke, M. J.; Schmidmaier, G. Local Delivery of Growth Factors Using Coated Suture Material. *Sci. World J.* **2012**, *2012*, 109216.

(15) Celiz, A. D.; Smith, J. G. W.; Langer, R.; Anderson, D. G.; Winkler, D. A.; Barrett, D. A.; Davies, M. C.; Young, L. E.; Denning, C.; Alexander, M. R. Materials for Stem Cell Factories of the Future. *Nat. Mater.* **2014**, *13*, 570–579.

(16) Marx, V. Cell Culture: A Better Brew. *Nature* **2013**, *496*, 253–258.

(17) Escobedo-Lucea, C.; Bellver, C.; Gandia, C.; Sanz-Garcia, A.; Esteban, F. J.; Mirabet, V.; Forte, G.; Moreno, I.; Lezameta, M.; Ayuso-Sacido, A.; *et al.* A Xenogeneic-Free Protocol for Isolation and Expansion of Human Adipose Stem Cells for Clinical Uses. *PLoS One* **2013**, *8*, e67870.

(18) Mosqueira, D.; Pagliari, S.; Uto, K.; Ebara, M.; Romanazzo, S.; Escobedo-Lucea, C.; Nakanishi, J.; Taniguchi, A.; Franzese, O.; Di Nardo, P.; *et al.* Hippo Pathway Effectors Control Cardiac Progenitor Cell Fate by Acting as Dynamic Sensors of Substrate Mechanics and Nanostructure. *ACS Nano* **2014**, *8*, 2033–2047.

(19) Dalby, M. J.; Gadegaard, N.; Oreffo, R. O. C. Harnessing Nanotopography and Integrin-Matrix Interactions to Influence Stem Cell Fate. *Nat. Mater.* **2014**, *13*, 558–569.

(20) Gerberich, B. G.; Bhatia, S. K. Tissue Scaffold Surface Patterning for Clinical Applications. *Biotechnol. J.* **2013**, *8*, 73–84.

(21) Faucheux, N.; Schweiss, R.; Lützow, K.; Werner, C.; Groth, T. Self-Assembled Monolayers with Different Terminating Groups as Model Substrates for Cell Adhesion Studies. *Biomaterials* **2004**, *25*, 2721–2730.

(22) Ahn, H. H.; Lee, I. W.; Lee, H. B.; Kim, M. S. Cellular Behavior of Human Adipose-Derived Stem Cells on Wettable Gradient Polyethylene Surfaces. *Int. J. Mol. Sci.* **2014**, *15*, 2075–2086.

(23) Klemm, D.; Kramer, F.; Moritz, S.; Lindström, T.; Ankerfors, M.; Gray, D.; Dorris, A. Nanocelluloses: A New Family of Nature-Based Materials. *Angew. Chem. Int. Ed. Engl.*

2011, *50*, 5438–5466.

(24) Iwamoto, S.; Kai, W.; Isogai, A.; Iwata, T. Elastic Modulus of Single Cellulose Microfibrils from Tunicate Measured by Atomic Force Microscopy. *Biomacromolecules* **2009**, *10*, 2571–2576.

(25) Saito, T.; Kuramae, R.; Wohlert, J.; Berglund, L. A.; Isogai, A. An Ultrastrong Nanofibrillar Biomaterial: The Strength of Single Cellulose Nanofibrils Revealed via Sonication-Induced Fragmentation. *Biomacromolecules* **2013**, *14*, 248–253.

(26) Eichhorn, S. J.; Dufresne, A.; Aranguren, M.; Marcovich, N. E.; Capadona, J. R.; Rowan, S. J.; Weder, C.; Thielemans, W.; Roman, M.; Renneckar, S.; *et al. Review: Current International Research into Cellulose Nanofibres and Nanocomposites*; 2010; Vol. 45.

(27) Shopsowitz, K. E.; Qi, H.; Hamad, W. Y.; Maclachlan, M. J. Free-Standing Mesoporous Silica Films with Tunable Chiral Nematic Structures. *Nature* **2010**, *468*, 422–425.

(28) Korhonen, J. T.; Hiekkataipale, P.; Malm, J.; Karppinen, M.; Ikkala, O.; Ras, R. H. a. Inorganic Hollow Nanotube Aerogels by Atomic Layer Deposition onto Native Nanocellulose Templates. *ACS Nano* **2011**, *5*, 1967–1974.

(29) Pääkkö, M.; Vapaavuori, J.; Silvennoinen, R.; Kosonen, H.; Ankerfors, M.; Lindström, T.; Berglund, L. a.; Ikkala, O. Long and Entangled Native Cellulose I Nanofibers Allow Flexible Aerogels and Hierarchically Porous Templates for Functionalities. *Soft Matter* **2008**, *4*, 2492.

(30) Henriksson, M.; Berglund, L. a; Isaksson, P.; Lindström, T.; Nishino, T. Cellulose Nanopaper Structures of High Toughness. *Biomacromolecules* **2008**, *9*, 1579–1585.

(31) Wang, M.; Anoshkin, I. V; Nasibulin, A. G.; Korhonen, J. T.; Seitsonen, J.; Pere, J.; Kauppinen, E. I.; Ras, R. H. A.; Ikkala, O. Modifying Native Nanocellulose Aerogels with Carbon Nanotubes for Mechanoresponsive Conductivity and Pressure Sensing. *Adv. Mater.* **2013**, *25*, 2428–2432.

(32) Wang, M.; Olszewska, A.; Walther, A.; Malho, J.-M.; Schacher, F. H.; Ruokolainen, J.; Ankerfors, M.; Laine, J.; Berglund, L. A.; Osterberg, M.; *et al.* Colloidal Ionic Assembly between Anionic Native Cellulose Nanofibrils and Cationic Block Copolymer Micelles into Biomimetic Nanocomposites. *Biomacromolecules* **2011**, *12*, 2074–2081.

(33) Walther, A.; Timonen, J. V. I.; Díez, I.; Laukkanen, A.; Ikkala, O. Multifunctional High-Performance Biofibers Based on Wet-Extrusion of Renewable Native Cellulose Nanofibrils. *Adv. Mater.* **2011**, *23*, 2924–2928.

(34) Iwamoto, S.; Isogai, A.; Iwata, T. Structure and Mechanical Properties of Wet-Spun Fibers Made from Natural Cellulose Nanofibers. *Biomacromolecules* **2011**, *12*, 831–836.

(35) Mathew, A. P.; Oksman, K.; Pierron, D.; Harmad, M.-F. Crosslinked Fibrous Composites Based on Cellulose Nanofibers and Collagen with in Situ pH Induced Fibrillation. *Cellulose* **2011**, *19*, 139–150.

(36) Eyholzer, C.; de Couraça, A. B.; Duc, F.; Bourban, P. E.; Tingaut, P.; Zimmermann, T.; Månson, J. A. E.; Oksman, K. Biocomposite Hydrogels with Carboxymethylated, Nanofibrillated Cellulose Powder for Replacement of the Nucleus Pulposus. *Biomacromolecules* **2011**, *12*, 1419–1427.

(37) Cherian, B. M.; Leão, A. L.; de Souza, S. F.; Costa, L. M. M.; de Olyveira, G. M.; Kottaisamy, M.; Nagarajan, E. R.; Thomas, S. Cellulose Nanocomposites with Nanofibres Isolated from Pineapple Leaf Fibers for Medical Applications. *Carbohydr. Polym.* **2011**, *86*, 1790–1798.

(38) Valo, H.; Arola, S.; Laaksonen, P.; Torkkeli, M.; Peltonen, L.; Linder, M. B.; Serimaa, R.; Kuga, S.; Hirvonen, J.; Laaksonen, T. Drug Release from Nanoparticles Embedded in Four Different Nanofibrillar Cellulose Aerogels. *Eur. J. Pharm. Sci.* **2013**, *50*, 69–77.

(39) Petersen, N.; Gatenholm, P. Bacterial Cellulose-Based Materials and Medical Devices: Current State and Perspectives. *Appl. Microbiol. Biotechnol.* **2011**, *91*, 1277–1286.

(40) Czaja, W.; Krystynowicz, A.; Bielecki, S.; Brown, R. M. Microbial Cellulose--the Natural Power to Heal Wounds. *Biomaterials* **2006**, *27*, 145–151.

(41) Bhattacharya, M.; Malinen, M. M.; Lauren, P.; Lou, Y.-R.; Kuisma, S. W.; Kanninen, L.; Lille, M.; Corlu, A.; GuGuen-Guillouzo, C.; Ikkala, O.; *et al.* Nanofibrillar Cellulose Hydrogel Promotes Three-Dimensional Liver Cell Culture. *J. Control. Release* **2012**, *164*, 291–298.

(42) Lou, Y.-R.; Kanninen, L.; Kuisma, T.; Niklander, J.; Noon, L. A.; Burks, D.; Urtti, A.; Yliperttula, M. The Use of Nanofibrillar Cellulose Hydrogel as a Flexible Three-Dimensional Model to Culture Human Pluripotent Stem Cells. *Stem Cells Dev.* **2014**, *23*, 380–392.

(43) Malinen, M. M.; Kanninen, L. K.; Corlu, A.; Isoniemi, H. M.; Lou, Y.-R.; Yliperttula, M. L.; Urtti, A. O. Differentiation of Liver Progenitor Cell Line to Functional Organotypic Cultures in 3D Nanofibrillar Cellulose and Hyaluronan-Gelatin Hydrogels. *Biomaterials* **2014**, *35*, 5110–5121.

(44) Markstedt, K.; Mantas, A.; Tournier, I.; Martínez Ávila, H.; Hägg, D.; Gatenholm, P. 3D Bioprinting Human Chondrocytes with Nanocellulose-Alginate Bioink for Cartilage Tissue Engineering Applications. *Biomacromolecules* **2015**, *16*, 1489–1496.

(45) Schneider, C. A.; Rasband, W. S.; Eliceiri, K. W. NIH Image to ImageJ: 25 Years of Image Analysis. *Nat. Methods* **2012**, *9*, 671–675.

(46) Håkansson, K. M. O.; Fall, A. B.; Lundell, F.; Yu, S.; Krywka, C.; Roth, S. V; Santoro, G.; Kvick, M.; Prahl Wittberg, L.; Wågberg, L.; *et al.* Hydrodynamic Alignment and Assembly of Nanofibrils Resulting in Strong Cellulose Filaments. *Nat. Commun.* **2014**, *5*, 4018.

(47) Torres-Rendon, J. G.; Schacher, F. H.; Ifuku, S.; Walther, A. Mechanical Performance of Macrofibers of Cellulose and Chitin Nanofibrils Aligned by Wet-Stretching: A Critical Comparison. *Biomacromolecules* **2014**, *15*, 2709–2717.

(48) Malho, J.-M.; Laaksonen, P.; Walther, A.; Ikkala, O.; Linder, M. B. Facile Method for Stiff, Tough, and Strong Nanocomposites by Direct Exfoliation of Multilayered Graphene into Native Nanocellulose Matrix. *Biomacromolecules* **2012**, *13*, 1093–1099.

(49) Hooshmand, S.; Aitomäki, Y.; Norberg, N.; Mathew, A. P.; Oksman, K. Dry-Spun Single-Filament Fibers Comprising Solely Cellulose Nanofibers from Bioresidue. *ACS Appl. Mater. Interfaces* **2015**, *7*, 13022–13028.

(50) Xu, G. G.; Yang, C. Q.; Deng, Y. Applications of Bifunctional Aldehydes to Improve Paper Wet Strength. *J. Appl. Polym. Sci.* **2002**, *83*, 2539–2547.

(51) Woo, S. .-Y.; Levine, R. E. Ligament, Tendon and Fascia. In *Handbook of Biomaterial Properties SE - 6*; Black, J.; Hastings, G., Eds.; Springer US, 1998; pp. 59–65.

(52) Zuk, P. A.; Zhu, M.; Ashjian, P.; De Ugarte, D. A.; Huang, J. I.; Mizuno, H.; Alfonso, Z. C.; Fraser, J. K.; Benhaim, P.; Hedrick, M. H. Human Adipose Tissue Is a Source of Multipotent Stem Cells. *Mol. Biol. Cell* **2002**, *13*, 4279–4295.

(53) Singelyn, J. M.; Christman, K. L. Modulation of Material Properties of a Decellularized Myocardial Matrix Scaffold. *Macromol. Biosci.* **2011**, *11*, 731–738.

(54) Huang-Lee, L. L.; Cheung, D. T.; Nimni, M. E. Biochemical Changes and Cytotoxicity Associated with the Degradation of Polymeric Glutaraldehyde Derived Crosslinks. *J. Biomed. Mater. Res.* **1990**, *24*, 1185–1201.

(55) Desbordes, S. C.; Placantonakis, D. G.; Ciro, A.; Socci, N. D.; Lee, G.; Djaballah, H.; Studer, L. High-Throughput Screening Assay for the Identification of Compounds Regulating Self-Renewal and Differentiation in Human Embryonic Stem Cells. *Cell Stem Cell* **2008**, *2*, 602–612.

(56) Arruda, A. P.; Pers, B. M.; Parlakgül, G.; Güney, E.; Inouye, K.; Hotamisligil, G. S. Chronic Enrichment of Hepatic Endoplasmic Reticulum-Mitochondria Contact Leads to Mitochondrial Dysfunction in Obesity. *Nat. Med.* **2014**, *20*, 1427–1435.

(57) Escribá, M.-J.; Escobedo-Lucea, C.; Mercader, A.; de los Santos, M.-J.; Pellicer, A.; Remohí, J. Ultrastructure of Preimplantation Genetic Diagnosis-Derived Human Blastocysts Grown in a Coculture System after Vitrification. *Fertil. Steril.* **2006**, *86*, 664–671.

(58) Gerecht, S.; Burdick, J. A.; Ferreira, L. S.; Townsend, S. A.; Langer, R.; Vunjak-Novakovic, G. Hyaluronic Acid Hydrogel for Controlled Self-Renewal and Differentiation of Human Embryonic Stem Cells. *Proc. Natl. Acad. Sci. U. S. A.* **2007**, *104*, 11298–11303.

(59) Doorn, J.; Moll, G.; Le Blanc, K.; van Blitterswijk, C.; de Boer, J. Therapeutic Applications of Mesenchymal Stromal Cells: Paracrine Effects and Potential Improvements. *Tissue Eng. Part B. Rev.* **2012**, *18*, 101–115.

(60) Dalamaga, M.; Diakopoulos, K. N.; Mantzoros, C. S. The Role of Adiponectin in Cancer: A Review of Current Evidence. *Endocr. Rev.* **2012**, *33*, 547–594.

(61) Smith, H. W.; Marshall, C. J. Regulation of Cell Signalling by uPAR. *Nat. Rev. Mol. Cell Biol.* **2010**, *11*, 23–36.

(62) Almine, J. F.; Wise, S. G.; Hiob, M.; Singh, N. K.; Tiwari, K. K.; Vali, S.; Abbasi, T.; Weiss, A. S. Elastin Sequences Trigger Transient Proinflammatory Responses by Human

Dermal Fibroblasts. *FASEB J.* **2013**, *27*, 3455–3465.

(63) Escobedo-Lucea, C.; Ayuso-Sacido, A.; Xiong, C.; Prado-López, S.; del Pino, M. S.; Melguizo, D.; Bellver-Estellés, C.; Gonzalez-Granero, S.; Valero, M. L.; Moreno, R.; *et al.* Development of a Human Extracellular Matrix for Applications Related with Stem Cells and Tissue Engineering. *Stem Cell Rev.* **2012**, *8*, 170–183.

Figures

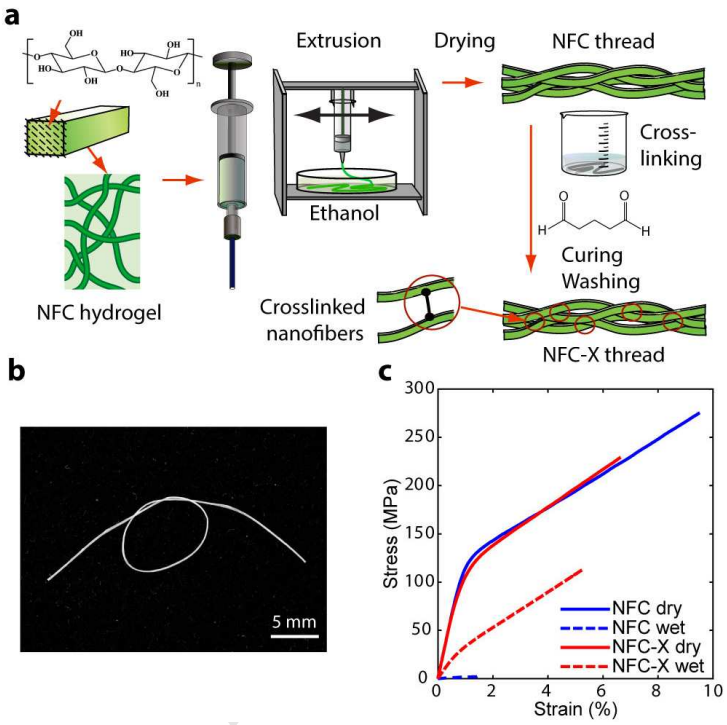

Figure 1

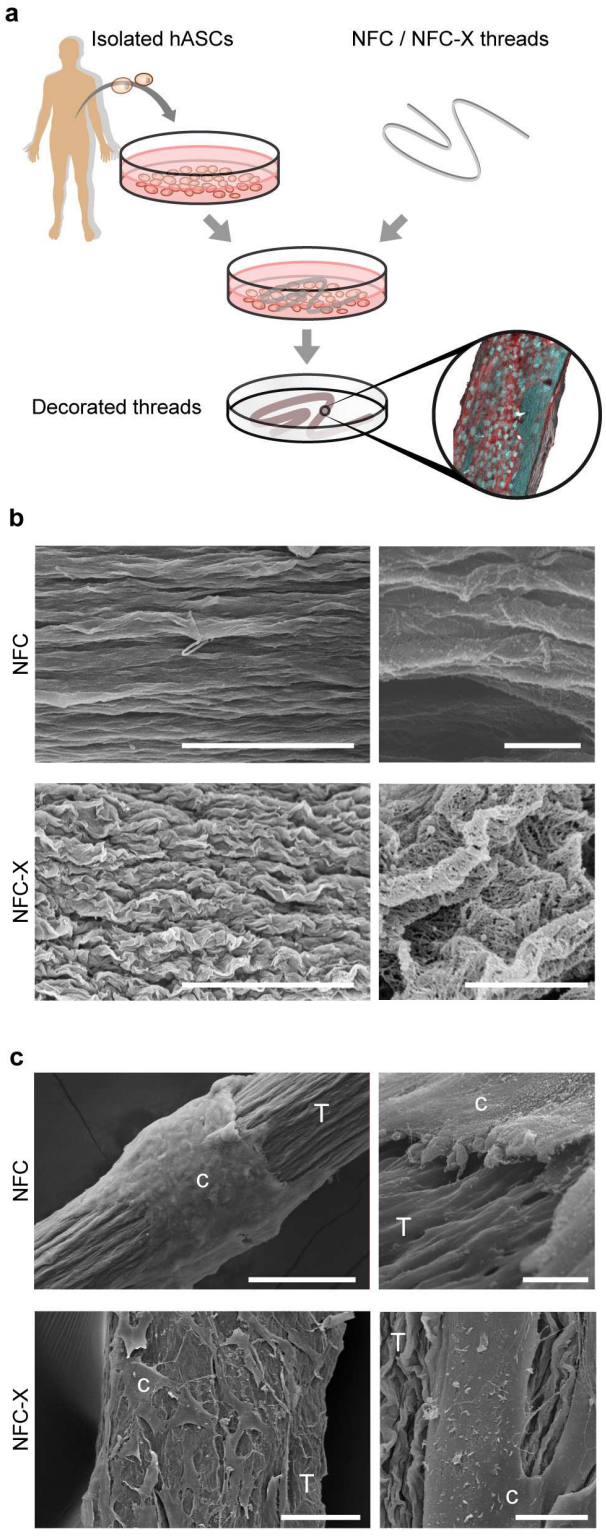
a
Isolated hASCs
NFC / NFC-X threads
Decorated threads
b
NFC
NFC-X
c
NFC
NFC-X
T
c

Figure 2

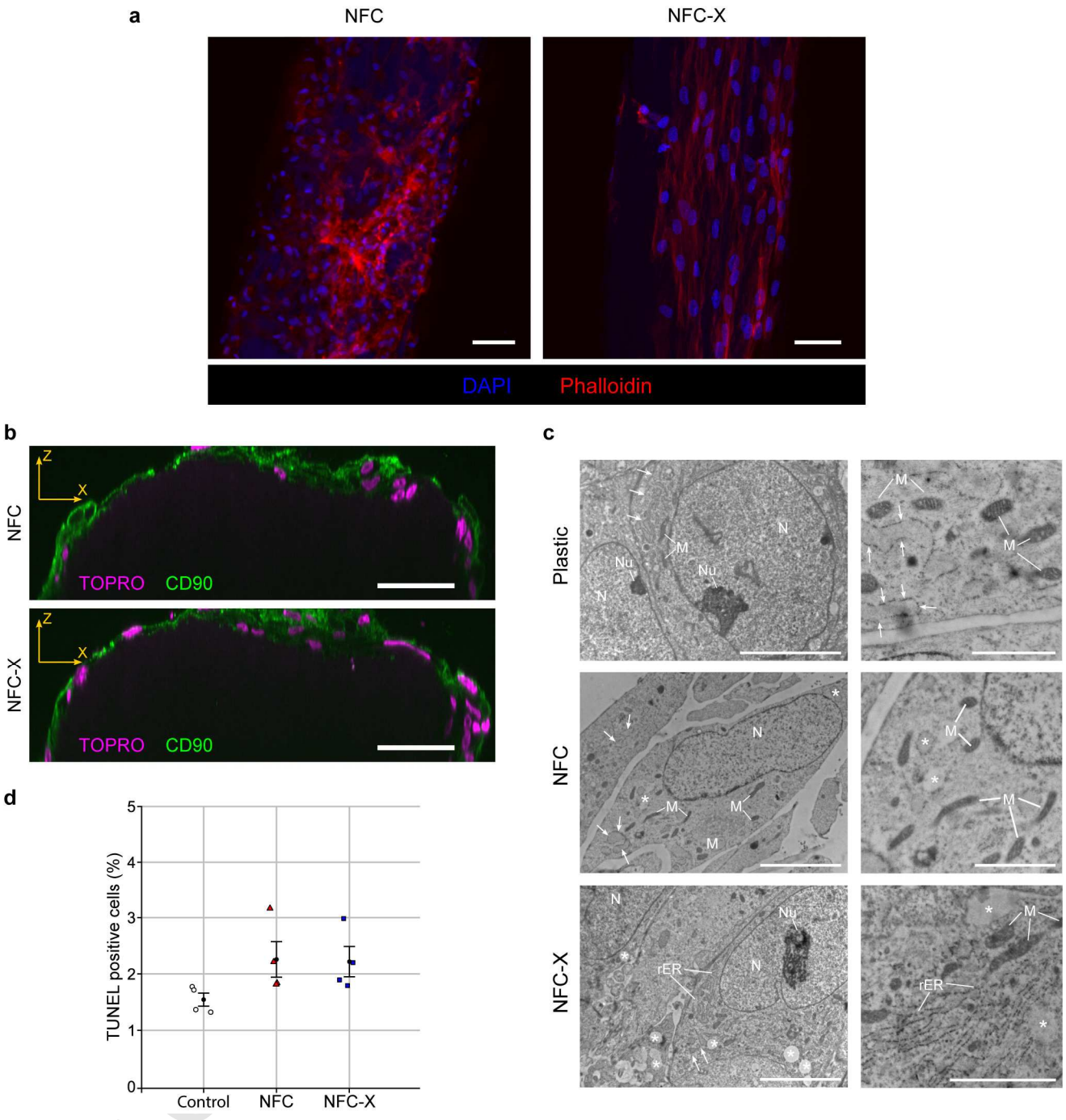
a
NFC
NFC-X
DAPI
Phalloidin
b
NFC
NFC-X
Z
X
TOPRO
CD90
c
Plastic
NFC
NFC-X
N
Nu
M
rER
d
TUNEL positive cells (%)
0
1
2
3
4
5
Control
NFC
NFC-X

Figure 3

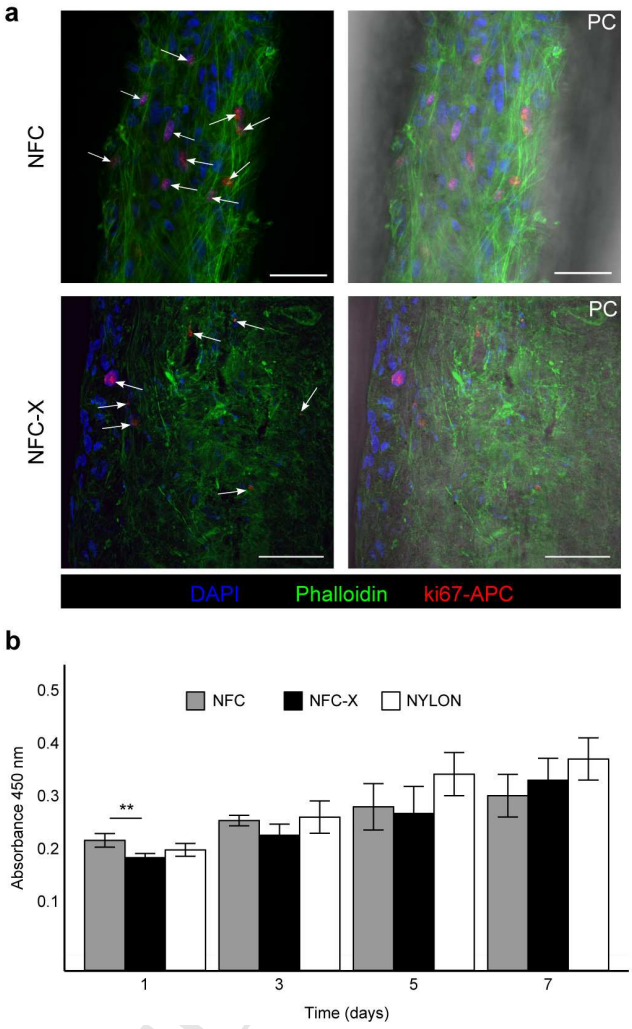

Figure 4

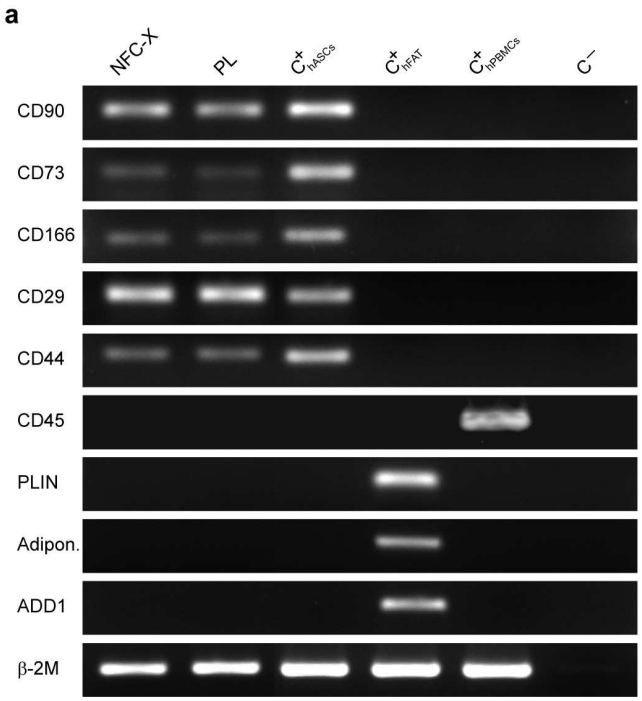
a
NFC-X
PL
C+ hASCs
C+ hFAT
C+ hPBMCs
C−
CD90
CD73
CD166
CD29
CD44
CD45
PLIN
Adipon.
ADD1
β-2M

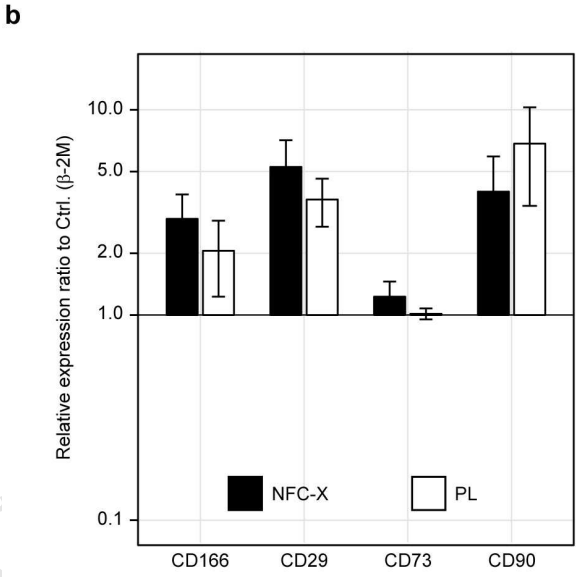
b
Relative expression ratio to Ctrl. (β-2M)
10.0
5.0
2.0
1.0
0.1
NFC-X
PL
CD166
CD29
CD73
CD90

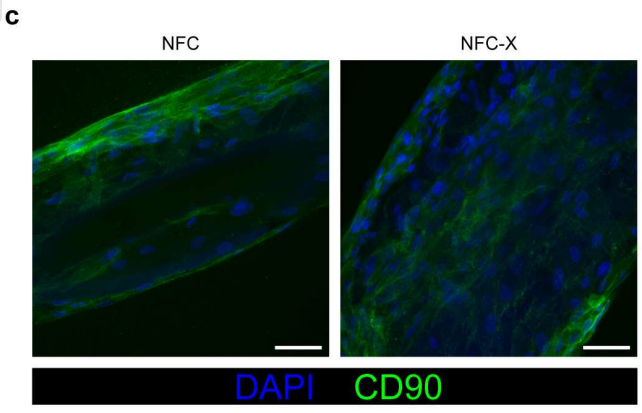
c
NFC
NFC-X
DAPI
CD90

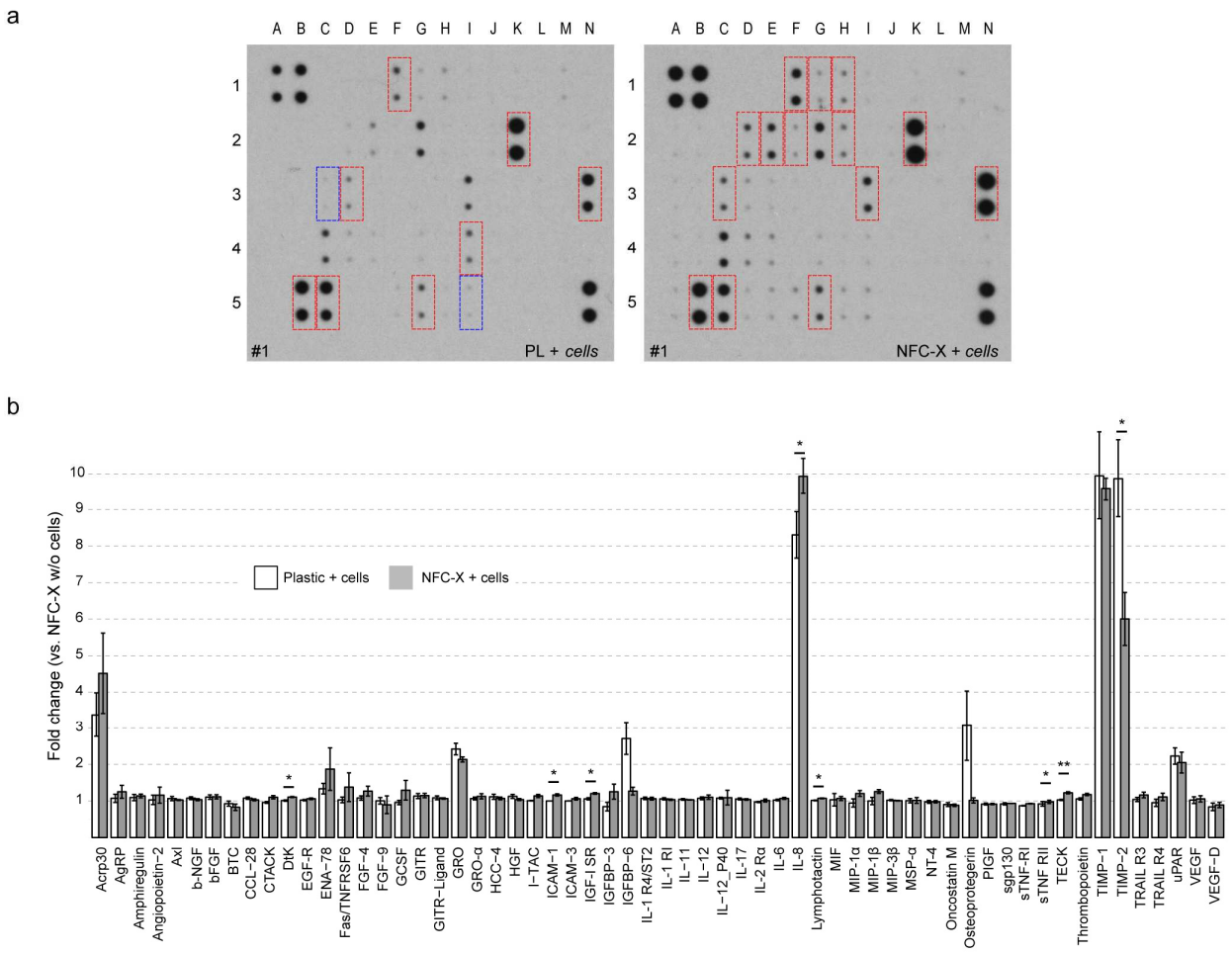

Figure 6

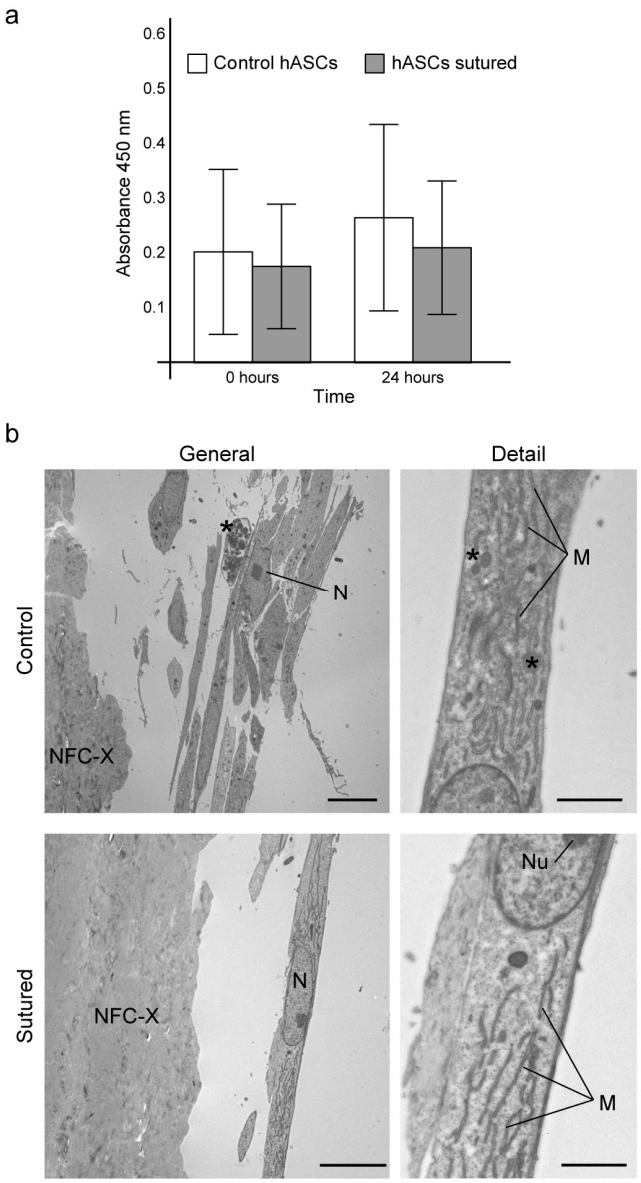
a
Control hASCs
hASCs sutured
Absorbance 450 nm
0.6
0.5
0.4
0.3
0.2
0.1
0 hours
24 hours
Time
b
General
Detail
Control
Sutured
NFC-X
N
M
Nu

Figure 7

Figure Captions and Tables

Figure 1. (**a)** Schematics for the preparation of NFC threads and their cross-linking with glutaraldehyde for NFC-X threads. (**b**) Photograph of a NFC thread. (**c**) Tensile stress-strain curves for NFC and NFC-X threads in dry state and soaked in water for 24h.

Figure 2. (a) Schematics illustrating the process to decorate NFC and NFC-X threads with hASC. **(b)** SEM images of the surface of NFC and NFC-X before seeding the cells. Scale bars 50 µm (left) and 2 µm (right). **(c)** SEM images showing cell adhesion and growth on NFC and NFC-X. The distribution of cells on NFC is non-homogeneous, whereas on NFC-X, the cells assume an elongated shape characteristic of mesenchymal cells. Labels: T, thread; c, cells. Scale bars 100 µm (left) and 10 µm (right).

Figure 3. (a) Immunocytochemistry shows the attachment of the cells on the thread surface. Especially on NFC-X, hASC exhibit elongated cytoplasmic intermediate filaments (stained red with phalloidin). Nuclei were counterstained in blue with DAPI. Scale bars 50 µm. **(b)** Transversal projection shows the distribution of the cells along the thread surface. Cell cytoplasm was stained against CD90 (green) to evidence the undifferentiated status. Nuclei were counterstained with TOPRO® (magenta). Scale bars 50 µm. **(c)** Representative TEM images of hASC cultured on plastic, over NFC and on NFC-X for one week, showing the absence of toxicity signs. Right images (scale bars 2 µm) are magnifications of the left images (scale bars 5 µm). Labels: M, mitochondrion; N, nucleus; Nu, nucleoli; rER, rough endoplasmic reticulum;*, lipid droplet; arrow, smooth endoplasmic reticulum. **(d)** TUNEL labeling assay shows a low overall level of apoptosis, indicating that the chemical cross-linking does not induce toxicity on the threads (n= 4 hASC lines). Data are shown as mean ± SEM.

Figure 4. (a) Immunocytochemistry against ki-67 demonstrating the presence of cells proliferating over NFC and NFC-X sutures. Fluorescent APC conjugated Ki-67 (red) expressed in the nuclei of mitotic cells. Actin filaments in the cytoplasm have been stained with phalloidin (green). Nuclei appear counterstained with DAPI (blue). Scale bars 50 µm. **(b)** Metabolic activity of NFC and NFC-X decorated sutures during one week in culture.

Figure 5. (a) RT-PCR data showing the expression of undifferentiated mesenchymal stem cell markers (CD90, CD73, CD166, CD29, CD44). Differentiation markers for the hematopoietic gene CD45 and the adipocyte-associated genes PLIN, adiponectin and ADD1 were checked, with negative results. hASC cultured on plastic (Pl) were used as a control, and beta-2-microglobulin (B2M) as control gene. cDNA from different human tissues was also included as positive controls for the different genes analyzed. Human mature fat (hFAT) for adipocyte differentiation markers; human peripheral blood mononuclear cells (hPBMC) for CD45, and undifferentiated hASC. (b) RT-qPCR comparing the expression levels of CD90, CD73, CD29 and CD166 in hASC cultured over plastic (Pl) and over NFC-X **(c)** Fluorescent CD90 labeling (green) shows the undifferentiated hASC on the thread surface. Nuclei have been counterstained in blue with DAPI. Scale bars 50 µm.

Figure 6. (a) Human cytokine antibody arrays were performed to compare the cytokine levels of the supernatant media seeded over plastic and on NFC-X. Four different conditions were studied: NFC-X without cells (Figure S10b); hASC seeded over plastic (left) and over NFC-X (right); and plastic without cells (Figure S10b). The factors that decreased or increased considerably are highlighted with blue or red boxes, respectively. The corresponding coordinates of the expressed cytokines are as follows: Acrp30 (1F), AgRP (1G), Angiopoietin-2 (1H), ENA-78 (2D), Fas/TNRSF6 (2E), FGF-4 (2F), GRO (2K), GCSF (2H), IGFBP-3 (3C), IGFBP-6 (3D), IL12-

p40 (3I), IL-8 (3N), Osteoprotegerin (4I), TIMP-1 (5B), TIMP-2 (5C), uPAR (5G), VEGF-D (5I). (See the full layout of the array in Figure S11). The functions of the cytokines as well as their identities are detailed in Table S2. Three independent experiments using 2 pools of two different hASC lines each one (6 in total) were performed (See the additional arrays in Figure S10b). **(b)** A chart representing the relative integrated densities of cytokine expression spots with respect to NFC-X without cells. Plastic with cells is marked in white, and NFC-X with cells in grey (n=3).

Figure 7. (a) Cell survival and morphology after suturing with NFC-X decorated threads. To evaluate the effect of mechanical stress during suturing, metabolic activity of decorated NFC-X sutures was determined after suturing in an ex vivo model using pig skin and compared with the metabolic levels expressed in control sutures seeded and maintained in the same conditions. No significant differences were observed immediately after the procedure or 24 hours later. **(b)** Comparison between the morphology of the cells remaining in the suture after the ex vivo experiments and the corresponding controls. The cell density is lower in the samples used for the suturing but cell morphology is similar in both conditions. The cytoplasm is rich in elongated mitochondria (M) characteristic functional and metabolic active cells and contains also few lipid droplets (*). No evidences of vacuoles or pyknosis suggesting cell death were detected. Nu= Nucleoli; N= nuclei. Scale bars in images: 10 µm (left) and 2 µm (right).

Table 1. Mechanical properties of NFC and NFC-X threads in dry state or soaked in water.

Sample	Tensile strength (MPa)	Strain at break (%)	Elastic modulus (GPa)	Modulus of toughness (MJ m^{-3})
NFC dry	275 ± 25	9.5 ± 1.0	13.1 ± 1.1	17.9 ± 3.2
NFC wet	2.0 ± 0.6	1.4 ± 0.2	0.20 ± 0.05	0.02 ± 0.01
NFC-X dry	227 ± 29	6.6 ± 1.2	13.1 ± 2.0	10.5 ± 2.7
NFC-X wet	111 ± 20	5.2 ± 1.2	4.0 ± 0.6	3.4 ± 1.3

Supplementary data

Figures S1-S11, Tables S1-S2, and Videos S1-S7.